

10-2010

Nanometer To Millimeter Scale Peptide-porphyrin Materials

Daniil V. Zaytsev

Fei Xie


Madhumita Mukherjee

Alexey Bludin

Borries Demeler

See next page for additional authors

Follow this and additional works at: https://scholarworks.bgsu.edu/chem_pub

 Part of the [Chemistry Commons](#)

Repository Citation

Zaytsev, Daniil V.; Xie, Fei; Mukherjee, Madhumita; Bludin, Alexey; Demeler, Borries; Breece, Robert M.; Tierney, David L.; and Ogawa, Michael Y., "Nanometer To Millimeter Scale Peptide-porphyrin Materials" (2010). *Chemistry Faculty Publications*. 124.
https://scholarworks.bgsu.edu/chem_pub/124

This Article is brought to you for free and open access by the Chemistry at ScholarWorks@BGSU. It has been accepted for inclusion in Chemistry Faculty Publications by an authorized administrator of ScholarWorks@BGSU.

Author(s)

Daniil V. Zaytsev, Fei Xie, Madhumita Mukherjee, Alexey Bludin, Borries Demeler, Robert M. Breece, David L. Tierney, and Michael Y. Ogawa

Nanometer to Millimeter Scale Peptide-Porphyrin Materials

Daniil V. Zaytsev,^{†,‡} Fei Xie,^{†,‡} Madhumita Mukherjee,[‡] Alexey Bludin,[‡] Borries Demeler,[§] Robert M. Breece,^{||} David L. Tierney,^{||} and Michael Y. Ogawa^{*,‡}

Department of Chemistry and Center for Photochemical Sciences, Bowling Green State University, Bowling Green, Ohio 43403, Center for Analytical Ultracentrifugation of Macromolecular Assemblies, University of Texas Health Science Center, San Antonio, Texas 78229, Department of Chemistry and Biochemistry, Miami University, Oxford, Ohio 45056

Received May 18, 2010; Revised Manuscript Received August 11, 2010

AQ-Pal14 is a 30-residue polypeptide that was designed to form an α -helical coiled coil that contains a metal-binding 4-pyridylalanine residue on its solvent-exposed surface. However, characterization of this peptide shows that it exists as a three-stranded coiled coil, not a two-stranded one as predicted from its design. Reaction with cobalt(III) protoporphyrin IX (Co-PPIX) produces a six-coordinate Co-PPIX(AQ-Pal14)₂ species that creates two coiled-coil oligomerization domains coordinated to opposite faces of the porphyrin ring. It is found that this species undergoes a buffer-dependent self-assembly process: nanometer-scale globular materials were formed when these components were reacted in unbuffered H₂O, while millimeter-scale, rod-like materials were prepared when the reaction was performed in phosphate buffer (20 mM, pH 7). It is suggested that assembly of the globular material is dictated by the conformational properties of the coiled-coil forming AQ-Pal14 peptide, whereas that of the rod-like material involves interactions between Co-PPIX and phosphate ion.

Introduction

The design of supramolecular materials entails the use of noncovalent interactions to guide the organization of discrete molecular subunits into forming structures of added complexity. Polypeptides are likely building blocks for preparing such materials because of their ability to utilize optimal combinations of hydrogen bond, electrostatic, and hydrophobic interactions in the self-assembly of robust structural motifs. Because of this, the design of supramolecular peptide-based materials has been the focus of much interest,^{1–4} making important contributions to such diverse areas of study as tissue engineering,⁵ drug delivery,⁶ and the design of stimuli-responsive materials.⁷ Inspired by this work, we^{8–13} and others^{14–21} have sought to expand the synthetic toolbox employed in the construction of such materials by exploring the use of transition metal chemistry to help direct the assembly of polypeptides and proteins in ways that may add to, and perhaps complement, the existing repertoire of native biological structures.²² This approach to “metal-mediated peptide assembly” thus exploits the directional bonding properties of inorganic coordination compounds to route the spatial orientation of polypeptides in ways that can yield new types of bioinspired materials for future applications in medicine and technology.

Our group has focused on preparing biological materials based on the self-assembling peptide structure of an α -helical coiled coil. This common protein structure motif exists as a left-handed supercoiling of two or more α -helices stabilized by a specific “knobs-into-holes” packing of hydrophobic side chains arising from its constituent peptides.²³ A considerable body of work has been performed during the last two decades to show that synthetic coiled coils can be prepared from peptide sequences

that are based on a seven-residue heptad repeat that is often labeled $(abcdefg)_n$.^{24–26} It has been found that if the heptad *a* and *d* positions are occupied by nonpolar amino acids, a hydrophobic face of the helix is created that can serve as a noncovalent oligomerization domain for the coiled coil. This assembly can be further enhanced by occupying positions *b*, *c*, and *f* with hydrophilic amino acids and by placing oppositely charged residues at positions *e* and *g* to create a network of stabilizing interhelix salt bridges. Seminal work by Harbury et al.²⁷ showed that the oligomerization states of these assemblies can be systematically changed by controlling the packing interactions that occur within their hydrophobic cores. Thus, coiled-coil dimers were formed when the heptad *a* and *d* positions of the GCN4 transcription factor were substituted by isoleucine and leucine, respectively, whereas tetramers were formed when the opposite substitutions (*a* = leucine, *d* = isoleucine) were made. Such observations formed the basis for a set of generally accepted guidelines for designing coiled coils having predetermined oligomerization states. However, recent work by the Woolfson group²⁸ has suggested that the Harbury rules may not necessarily apply to synthetic coiled-coil sequences and that the observations giving rise to these rules may be sequence context-dependent. Results presented below will show that this is indeed true for the system studied in this work.

In recent years, our group has sought to enhance the self-assembly properties of α -helical coiled coils by adding metal-binding sites to either their hydrophobic cores or their solvent-exposed surfaces. This work has shown that two distinct classes of peptide materials can be prepared from the approach of metal-mediated assembly. Discrete peptide assemblies can be prepared by binding metal ions to the hydrophobic interiors of coiled coils in which a Cys-X-X-Cys binding domain was introduced into a single heptad repeat of a coiled-coil forming peptide.^{11–13} In these systems, cysteine residues occupied the *a* and *d* positions of the third heptad repeat, which completely disrupted the coiled-coil structure. However, subsequent metal coordination was found to reorganize the peptide into creating metal-

* To whom correspondence should be addressed. E-mail: mogawa@bgsu.edu.

[†] These authors contributed equally to this work.

[‡] Bowling Green State University.

[§] University of Texas Health Science Center.

^{||} Miami University.

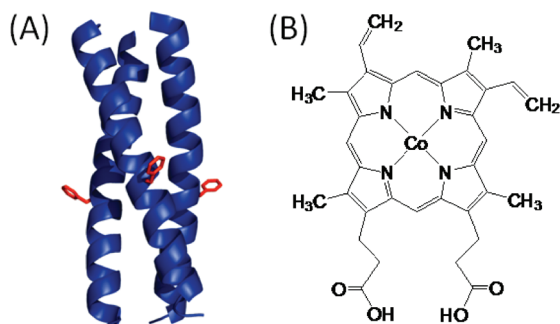


Figure 1. Peptide and porphyrin components used in this study consisting of (A) the AQ-Pal14 coiled-coil trimer shown as a computer-generated model and (B) Co-PPIX.

peptide assemblies that can be regarded as being model metalloproteins whose spatial dimensions are on the order of several nanometers. Other work by our group has shown that extended assemblies can be designed by placing metal-binding sites at the solvent-exposed surfaces of self-assembling coiled-coil structures.^{8–10} Most recently, a polypeptide called AQ-Pal14, which was thought to form two-stranded α -helical coiled coils, but now is shown to form trimeric coiled coils (vide infra), was derivatized with a metal-binding 4-pyridylalanine (Pal) site at its surface. These were then coordinated to the *cis* positions of a Pt(ethylenediamine) metal center to produce a Pt-peptide tecton unit in which two coiled-coil forming peptides are oriented at right angles from each other within the metal complex. It was found that oligomerization of these metal-peptide tectons by interunit coiled-coil formation results in the production of a heterogeneous population of globular and fibrillar assemblies having dimensions on the order of 10–100 nm.⁸ It was speculated that the different morphologies of these assemblies could result from the coordination geometry of the metal complex used in their formation.

The work to be described below will show how the coordination of the same coiled-coil forming AQ-Pal14 polypeptide to the axial positions of Co-PPIX (Figure 1) results in the construction of Co-PPIX(AQ-Pal14)₂ tectons in which peptide coordination occurs at opposite faces of the porphyrin ring. Circular dichroism spectroscopy, size exclusion chromatography, and dynamic light scattering measurements show that the Co-PPIX/AQ-Pal14 tectons do indeed self-assemble through coiled-coil formation in solution to produce structures having a mean hydrodynamic radius of about 50 nm. When deposited onto a solid support from unbuffered H₂O, atomic force microscopy shows that these materials assume a conical morphology having a base diameter about 40–80 nm, consistent with the light scattering results. The similarity of these structures to those formed by the Pt/AQ-Pal14 indicates that their morphologies are dictated by the conformational properties of the peptide component and not their constituent metal complexes. Interestingly, when these materials are prepared from phosphate buffer, a second type of material is formed that is visible to the naked eye and consists of rod-like structures having millimeter-scale lengths and micrometer-scale diameters. These structures are significantly larger and considerably more organized than those previously prepared by our group, and the results demonstrate the structural diversity of materials that can be prepared from peptidic and inorganic components.

Experimental Section

Synthetic Methods. The AQ-Pal14 peptide synthesis and purification were performed as previously described⁸ and analyzed by matrix-

assisted laser desorption ionization mass spectrometry (MALDI-MS: calcd for [M + H⁺], 3280.86; found, 3280.11). The metal-peptide assemblies were formed by combining 1 mM solution of AQ-Pal14 and 0.5 mM solution of Co-PPIX in 5:95 (v/v) DMF in 20 mM phosphate buffer (pH 7.0) and incubating at 60 °C for 2–24 h. Before microscopic analysis, the crude reaction mixture was washed with dichloromethane to remove any unreacted Co-PPIX.

Raman and Infrared Spectroscopy. Raman spectroscopy experiments were performed on a Renishaw inVia Raman microscope with a 442 nm laser focused using a 50 \times objective lens. Micro ATR-FTIR spectroscopy experiments were performed on a Varian FTS4000 spectrometer coupled to a Varian UMA600 IR microscope.

Mass Spectrometry. MALDI-MS data was acquired on a Bruker Daltonics Omnistar time-of-flight spectrometer using the linear positive mode. The employed matrix solutions were saturated solutions of α -cyano-4-hydroxycinnamic acid, sinapinic acid or 6-aza-2-thiothymine in acetonitrile/H₂O (75:25, v/v). For analysis of the Co-PPIX/AQ-Pal14 materials, an individual rod was isolated from the SEM substrate and placed onto a MALDI target plate. This was then carefully washed with methanol to remove the outer layers of the material in an attempt to remove any unreacted starting materials from the sample before mixing with the matrix solution.

Size Exclusion Chromatography. Size exclusion chromatography (SEC) of the AQ-Pal14 apo-peptide were performed with simultaneous multiangle static light scattering (MALS) detection and dynamic light scattering (DLS) on a Superdex 75 10/300 GL Tricorn column equilibrated with 0.05–0.10 M phosphate buffer (pH 7.0) and 0.1–1 M KCl at a flow rate of 0.3–0.5 mL/min. The eluant was passed in a sequential order through a Shimadzu SPD-10AV UV-vis spectrophotometer, a Wyatt miniDAWN Tristar three-angle laser light scattering photometer coupled with a Wyatt DLS correlator at a 90° scattering angle, and a Wyatt Optilab rEX refractive index detector. Data collection and processing was carried out using Wyatt Astra software. Local concentrations for the eluting AQ-Pal14 fractions were calculated on the basis of a specific refractive index increment value, dn/dc , of 0.185 mL/g. The latter value was confirmed by measuring the refractive index changes in a series of peptide dilutions in 0.05 M potassium phosphate buffer, 0.10 M potassium chloride, pH 7.0. The apparent weight average molar mass M_w of the peptide was calculated using the Zimm fit method using a first-degree polynomial.

DLS data for the AQ-Pal14 SEC eluates was also collected simultaneously with MALS. The additional batch DLS experiments were performed on fresh AQ-Pal14 samples prepared in water or buffer media and filtered through 0.02 μ m filter. In DLS experiments, a correlation function $g^{(2)}(\tau)$ was recorded and analyzed using the method of cumulants²⁹ to yield the translational diffusion coefficient D . Alternatively, the correlation function data was processed using the regularization algorithm as implemented in Astra software to obtain a distribution plot of D values. The calculated value of D was corrected to standard conditions of water at 20 °C ($D_{20,w}$). Subsequently, the hydrodynamic radius R_h was found according to the Stokes–Einstein relation.

SEC experiments on the Co-PPIX/peptide reaction mixtures were performed using a Superdex 200 10/300 GL Tricorn column. The samples were eluted using 0.05 M potassium phosphate buffer, 0.1 M KCl, pH 7.0, at a flow rate of 0.4 mL/min and monitored at a wavelength of 256 nm. The injections of the Co-PPIX/AQ-Pal14 mixture were preceded by the control injections of buffer and then peptide only to ensure the cleanliness of a column and lack of shedding from the stationary phase. The eluted fractions were collected for further DLS analysis under a batch regime.

Analytical Ultracentrifugation Studies. Analytical ultracentrifugation (AUC) runs were performed on a Beckman Optima XLA analytical ultracentrifuge equipped with absorbance optics. AUC data processing was conducted using the UltraScan software. AQ-Pal14 samples were spun in six-channel centerpieces, using a Beckman An-60Ti rotor. In the sedimentation velocity (SV) experiments samples

were measured at 60 krpm at two loading concentrations (30 and 90 μM) in 20 mM phosphate buffer (pH 7.0) with ionic strength adjusted to 50 mM with NaCl, at 20 °C and monitored at 230 nm. The analysis of SV data involved the model-independent van Holde-Weischet analysis to obtain diffusion corrected distribution of sedimentation coefficient values (*s*-distribution). The limits of *s*-distribution were used to initialize the genetic algorithm (GA)³⁰ analysis and two-dimensional (2DSA)³¹ analysis to fit velocity scans with a finite element solution of the Lamm equation and thus obtain molecular parameters. The confidence intervals for corresponding parameters were estimated by the Monte Carlo approach as implemented in the Ultrascan software. Sedimentation equilibrium (SE) experiments were performed on two loading concentrations (60 and 90 μM) in 50 mM phosphate buffer (pH 7.0) with 100 mM KCl at 4 °C, using rotor speeds 40, 45, 50, 55, 60 krpm with monitoring at 235 nm ($\epsilon_{235} = 3850 \text{ M}^{-1} \text{ cm}^{-1}$). Equilibrium data were fit globally to multiple models using the Ultrascan software. The partial specific volume of the AQ-Pal14 peptide was calculated as the weighted average of tabulated data per amino acid residue and found to be 0.771 mL/g. In lieu of 4-pyridylalanine, phenylalanine was used to estimate the partial specific volume of AQ-Pal14. Predictions for the hydrodynamic properties of AQ-Pal14 in different oligomeric states were obtained using the SoMo bead modeling program³² incorporated within the Ultrascan software. The structural models for the appropriate oligomeric coiled-coil forms of AQ-Pal14 were generated from the GCN4 dimer (1ZIL), trimer (1ZIM) and tetramer (1GCL) structures according to the procedures described by Wagschal et al.³³

Scanning Electron Microscopy and Electron-Dispersive X-ray Analysis. SEM and EDX analyses were performed on an Inspect F scanning electron microscope (FEI Co., Hillsboro, OR) equipped with an INCAPentaFET-x3 detector from OXFORD Instruments. Samples were prepared by direct evaporation onto either carbon or copper conductive tapes under ambient conditions.

Atomic Force Microscopy. AFM analyses were performed using a Veeco Multimode Nanoscope IIIa atomic force microscope in tapping mode with BudgetSensors Tap300Al-G probes. A strip of freshly peeled muscovite mica was incubated in the sample solution for one day and then rinsed with distilled water and air-dried before imaging. The data were processed by WSxM 5.0 Develop 1.3 software.³⁴

X-ray Absorption Spectroscopy. Samples of Co-PPIX/AQ-Pal14 (~1 mM, including 20% (v/v) glycerol added as a glassing agent) was loaded in a Lucite cuvette with 6 μm polypropylene windows and frozen rapidly in liquid nitrogen. X-ray absorption spectra were measured at the National Synchrotron Light Source (NSLS), beamline X3B, with a Si(111) double crystal monochromator; harmonic rejection was accomplished using a Ni focusing mirror. Fluorescence excitation spectra were measured with a 13-element solid-state Ge detector array. Samples were held at ~15 K in a Displex cryostat during XAS measurements. X-ray energies were calibrated by reference to the absorption spectrum of a Co metal foil, measured concurrently. Data collection and reduction were performed according to published procedures³⁵ with E_0 set to 7735 eV. The Fourier-filtered EXAFS were fit to eq 1 using the nonlinear least-squares engine of IFEFFIT that is distributed with SixPack.³⁶ Fits to unfiltered data gave similar results.

$$\chi(k) = \sum \frac{N_{\text{as}} A_{\text{s}}(k) S_{\text{c}}}{k R_{\text{as}}^2} \exp(-2k^2 \sigma_{\text{as}}^2) \exp(-2R_{\text{as}}/\lambda) \sin[2k R_{\text{as}} + \phi_{\text{as}}(k)] \quad (1)$$

In eq 1, N_{as} is the number of scatterers within a given radius ($R_{\text{as}} \pm \sigma_{\text{as}}$), $A_{\text{s}}(k)$ is the backscattering amplitude of the absorber-scatterer (as) pair, S_{c} is a scale factor, $\phi_{\text{as}}(k)$ is the phase shift experienced by the photoelectron, λ is the photoelectron mean free-path, and the sum is taken over all shells of scattering atoms included in the fit. Theoretical amplitude and phase functions, $A_{\text{s}}(k) \exp(-2R_{\text{as}}/\lambda)$ and $\phi_{\text{as}}(k)$, were calculated using FEFF v. 8.³⁷ The scale factor ($S_{\text{c}} = 0.74$) and E_0 (26

eV) were determined previously³⁵ and held fixed throughout the fitting procedure, while refining only R_{as} and σ_{as}^2 for a given shell.

Results

Peptide Synthesis and Design. Solid phase methods were used to prepare the peptide AQ-Pal14, which has the sequence, Ac-Q-(IAALEQK)(IAALEXK)(IAALEQK)₂-G-NH₂, where X is the non-natural amino acid 4-pyridylalanine. The peptide was purified by reversed-phase HPLC and identified by MALDI mass spectrometry. As previously described,⁸ the sequence of AQ-Pal14 was designed to place a metal-binding pyridine site at a solvent-exposed heptad *f* position and is comprised of four heptad repeats, each of which contains isoleucine at the heptad *a* positions and leucine at the heptad *d* positions. Thus, in accordance with the design principles of Harbury et al.²⁷ and consistent with previous predictions²⁴ for the closely related peptides (IAALEQK)_{*n*≥3}, the AQ-Pal14 peptide was expected to form two-stranded coiled coils.

Circular Dichroism Spectroscopy of AQ-Pal14. The circular dichroism (CD) spectrum of AQ-Pal14 has minima at 222 and 208 nm with a ratio of $[\theta]_{222}/[\theta]_{208} = 1.07$ (25 °C), indicating that AQ-Pal14 does indeed exist as α -helical coiled coils in aqueous solution.²⁶ Thermal denaturation studies (Supporting Information, Figure S1) show no evidence for a cooperative melting transition in the range of 5–95 °C, and the peptide is seen to undergo only about 38% decrease in ellipticity at the highest temperature. For comparison, the high thermal stability of AQ-Pal14 is similar to that reported by Su et al.³⁸ for comparably sized synthetic coiled coils, but is significantly greater than that of the H21 30-mer peptide previously studied by our group,³⁹ which is based on the (IEALEGK) heptad repeat.

Static and Dynamic Light Scattering Studies of AQ-Pal14. The oligomerization state of the AQ-Pal14 peptide was assessed in aqueous solution at neutral pH by SEC-MALS (Supporting Information, Figure S2). This technique provides a direct determination of the molecular weight of peptides and proteins and avoids errors inherent within conventional SEC calibration methods for determining molecular weights of nonglobular analytes.⁴⁰ The size exclusion chromatogram of the AQ-Pal14 peptide consists of a single symmetrical peak whose elution time was found to be constant in the studied range of loading concentrations (0.05–3 mM) and the ionic strength of the elution buffer (0.10–1.15 M). Calculation of the apparent weight average molar mass M_w of the peptide using the Zimm fit method yielded a value of 9.5 ± 0.1 kDa, as determined from an average of four separate experiments. Because the calculated molecular mass for the peptide trimer is 9.84 kDa, these results indicate that the AQ-Pal14 peptide exists as a trimeric species under the conditions studied. This result is in contrast to the original expectation that the peptide would form a two-stranded coiled coil based on its sequence.

The hydrodynamic size of AQ-Pal14 at pH 7 was further assessed by DLS analysis performed in both batch and SEC-coupled modes. The distribution analysis of the autocorrelation function using the method of cumulants yielded a narrow, unimodal distribution of species having a mean value of the translational diffusion coefficient, $D_{20,w}$, equal to $(1.23 \pm 0.10) \times 10^{-6} \text{ cm}^2/\text{s}$. This corresponds to a hydrodynamic radius of 1.7 ± 0.1 nm. The regularization processing of the DLS data shows a similar estimation in the produced R_h distribution histogram which displays a narrow distribution centered at 1.7 nm (Supporting Information, Figure S3). This estimation of the hydrodynamic size is in very good agreement with the results

Table 1. Summary of Solution Studies of the Apo AQ-Pal14 Peptide at pH 7

		peptide concentration, μM	$s_{20,w}, \times 10^{-13}$ s	$D_{20,w}, \times 10^{-6}$ cm ² /s	f/f_0	R_h , nm	M_w , kDa
sedimentation velocity	GA - Monte Carlo	90	1.10	1.19	1.25	1.80	9.81
		30	1.10	1.22	1.23	1.76	9.57
	2DSA - Monte Carlo	90	1.11	1.19	1.25	1.81	9.90
		30	1.11	1.21	1.24	1.78	9.73
sedimentation equilibrium	single-component model	60; 90	n/a	n/a	n/a	n/a	8.89
	monomer-trimer model	60; 90	n/a	n/a	n/a	n/a	3.04 ^a
SEC-MALS		50–1000	n/a	n/a	n/a	n/a	9.50
DLS		300–1000	n/a	1.23	n/a	1.74	n/a
SoMo bead modeling ^b		n/a	1.14	1.22	1.22	1.75	n/a

^a The MW value is calculated for trimer. The fitted association constant is $6 \times 10^{11} \text{ M}^{-1}$. ^b As obtained for a peptide trimer coiled-coil model.

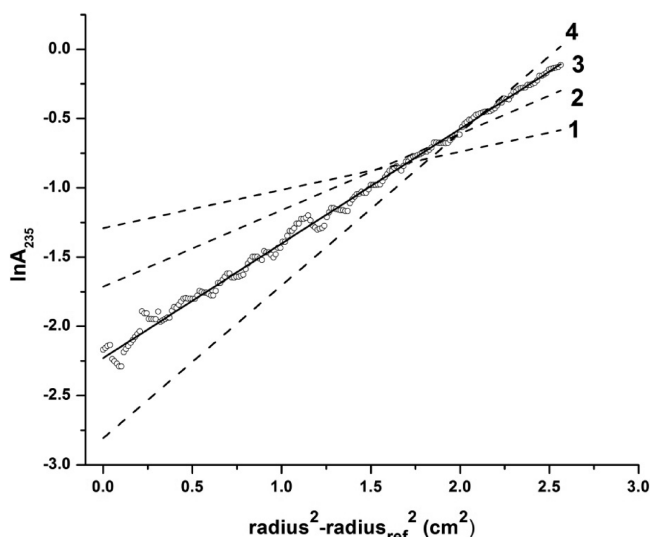


Figure 2. Sedimentation equilibrium of the AQ-Pal14 apopeptide. Calculated fits to a single-component model are shown for monomer (1), dimer (2), trimer (3), and tetramer (4).

of analytical ultracentrifugation experiments as described in the following section.

Analytical Ultracentrifugation Studies of AQ-Pal14. AUC experiments were used as a final means of determining the oligomerization state of the AQ-Pal14 peptide. Sedimentation velocity experiments were performed at loading concentrations of 30 and 90 μM AQ-Pal14. The fit of scans to the finite-element solutions of the Lamm equation using GA and 2DSA methods suggests the presence of a single major solute species of 9.57–9.90 kDa, which is consistent with the existence of a trimeric AQ-Pal14 species (Supporting Information, Figure S4). The obtained values of s and D along with M_w derived using the estimated specific partial volume of 0.771 mL/g are summarized in Table 1. Sedimentation equilibrium experiments were performed on AQ-Pal14 in the velocity range of 40–60 krpm and the corresponding equilibrium scans were best globally fit to a single-component model (variance of 8.4×10^{-5}) and monomer-trimer model (variance of 8.7×10^{-5}). The results of both fits (see Table 1) are indistinguishable from one another to indicate that AQ-Pal14 exists as a peptide trimer. Figure 2 shows a representative fit of the experimental scan to a single-species model. Shown are the experimental data trace for 60 μM AQ-Pal14 sedimented at 40 krpm (gray circles) and the fit to a trimeric single-species model (black line). Fits to monomeric, dimeric, and tetrameric masses in terms of single-species models (dashed lines) are shown for comparison. Additional equilibrium scans are presented in the Supporting Information, Figure S5.

In summary, MALS, sedimentation velocity, and equilibrium AUC experiments give identical results in determining that AQ-

Pal14 exists as peptide trimer in aqueous solution. The obtained hydrodynamic parameters for AQ-Pal14 are also in accordance with the theoretically derived $D_{20,w}$ and $s_{20,w}$ values as calculated for a bead model of AQ-Pal14 coiled-coil trimer using the SoMo program.³² It is noted that these results are consistent with our characterization of the cadmium adduct of a related peptide whose sequence is based on the IAALQK repeat but modified to contain metal binding cysteine residues at the *a* and *d* positions of the third heptad. Here, X-ray crystal studies show that the cadmium protein exists as a parallel three-stranded coiled-coil in which the presence of the metal site causes a distortion of the coiled-coil backbone.⁴¹ It thus appears that the Harbury rules for coiled-coil design are indeed context dependent as placement of isoleucine and leucine residues into the heptad *a* and *d* positions of the IAALQK repeat produces three-stranded coiled coils.

Binding of AQ-Pal14 to Co-PPIX. The binding of AQ-Pal14 to Co-PPIX was monitored by both UV–vis and CD spectroscopy. The successive addition of peptide to a solution of Co-PPIX at 60 °C results in a loss of intensity of the porphyrin Soret band that is accompanied by a distinct red-shift from 418 to 424 nm (Supporting Information, Figure S6). The porphyrin Q bands also undergo small red-shifts to 537 and 570 nm, respectively, upon the addition of peptide. These spectral changes are identical to those previously reported for the formation of [Co-PPIX(pyridine)₂] in alcohol solvents⁴² and indicate that the reaction of AQ-Pal14 with Co-PPIX results in the formation of a six-coordinate Co-PPIX(AQ-Pal14)₂ species in which two separate AQ-Pal14 peptides are bound to the axial positions of Co-PPIX. These results indicate formation of the desired metal-peptide tecton units in which two coiled-coil oligomerization domains are placed on opposite sides of the cobalt porphyrin ring. However, attempts to characterize this species by MALDI-MS were unsuccessful, showing only the presence of monomeric AQ-Pal14 and Co-PPIX species. This behavior might be due to the weakness of the peptide-porphyrin coordinate bond as suggested by the EXAFS results described below.

Further evidence for the binding of AQ-Pal14 to Co-PPIX can be seen in the CD spectrum of the peptide-porphyrin reaction mixture, which displays an induced CD signal consisting of a minimum ellipticity at 417 nm and a maximum at 438 nm (Supporting Information, Figure S7). This split CD band is indicative of close electronic communication occurring between the porphyrin π -system and the chiral peptide environment and is reminiscent of those observed in some heme proteins⁴³ as well as in supramolecular assemblies of porphyrins and either amino acids^{44,45} or designed polypeptides.^{46–49} The far UV region in the CD spectrum of the peptide-porphyrin solution is dominated by features at 208 and 222 nm and has an ellipticity ratio of $[\theta]_{222}/[\theta]_{208} = 1.06$ which suggests the assembly of the

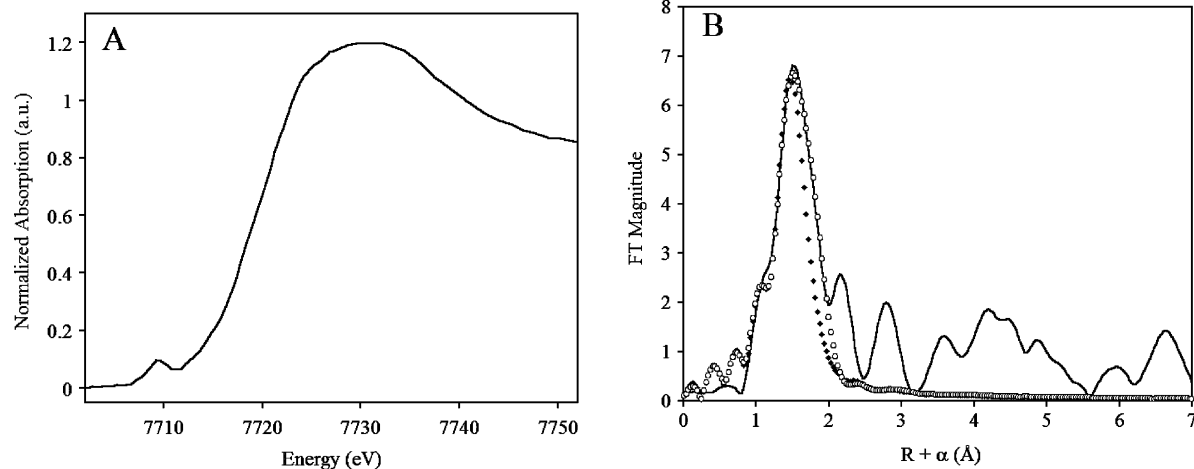


Figure 3. Normalized XANES (A) and EXAFS Fourier transform (B) for Co-PPIX/AQ-Pal14 (solid line) and corresponding fits for four pyrrole nitrogens (filled diamonds) and four pyrroles + two pyridine nitrogens (open circles).

Table 2. EXAFS Curve Fitting Results for Co-PPIX/AQ-Pal14^a

fit	model	Co-N _(porphyrin)	Co-N _(pyridine)	R_i^b	R_u^b
1	4 N _(porphyrin)	1.95 (1.6)		96	393
2	4 N _(porphyrin) + 2 N _(pyridine)	1.95 (2.0)	2.27 (3.6)	41	315

^a Distances (Å) and disorder parameters (in parentheses, σ^2 (10^{-3} Å²)) shown derive from integer or half-integer coordination number fits to Fourier filtered EXAFS data [$k = 1.5-12$ Å⁻¹; $R = 0.7-2$. Three Å]. ^b Goodness of fit (R_i for fits to filtered data; R_u for fits to unfiltered data) defined as $10^3 \times \frac{\sum_{i=1}^N \{[\text{Re}(\chi_i \text{ calc})]^2 + [\text{Im}(\chi_i \text{ calc})]^2\}}{\sum_{i=1}^N \{[\text{Re}(\chi_i \text{ obs})]^2 + [\text{Im}(\chi_i \text{ obs})]^2\}}$ where N is the number of data points.

metal-peptide tectons by interunit coiled-coil formation (Supporting Information, Figure S7).

Cobalt K-Edge XAS. To more fully define the coordination number of the cobalt center upon reaction with the peptide, X-ray absorption spectra were obtained for a solution of Co-PPIX/AQ-Pal14. The XANES spectrum (Figure 3A) shows an intense $1s \rightarrow 3d$ transition, consistent with low-spin Co(III) in a pseudo-octahedral environment. Similarly, the EXAFS curve fitting results (Table 2 and Figure 3B) indicate that the cobalt ion is indeed six-coordinate, with 4 Co-N_{pyrrole} bonds of 1.96 Å, in good agreement with those seen in other Co(III) porphyrinic systems.⁵⁰⁻⁵² Inclusion of a second set of two nitrogen scatterers within the primary coordination sphere leads to a 57% improvement in the fit residual (Supporting Information, Figure S8). This second set, corresponding to the axial pyridylalanine ligands, refines to a Co-N_{pyridine} distance of 2.27 Å. The axial ligand distance is longer than seen previously in isolated Co(III) porphyrins⁵¹ and Co-substituted myoglobin,^{50,52} and most likely reflects the added strain of the axial ligands' incorporation into the noncovalent assemblies. Significant multiple scattering from the porphyrin ring system is also apparent in the EXAFS data, but these interactions were not analyzed.

Supramolecular Assembly of the Co-PPIX/AQ-Pal14 Tectons. The supramolecular assembly of the Co-PPIX/AQ-Pal14 tectons was monitored by SEC on a Superdex 200 column. The bottom chromatogram in Figure 4 shows that the AQ-Pal14 peptide alone elutes as a single peak at about 17.3 mL. However, the SEC analysis of a freshly prepared mixture Co-PPIX/AQ-Pal14 (Figure 4, middle) results in the immediate formation of a new high molecular weight species that elutes at the column void volume (7.5 mL), which corresponds to a molecular mass of ≥ 600 kDa for globular analytes and ≥ 100 kDa for rod-shaped ones. This behavior is accompanied by the appearance of an intermediate-sized species with a broad nonsymmetrical distribution

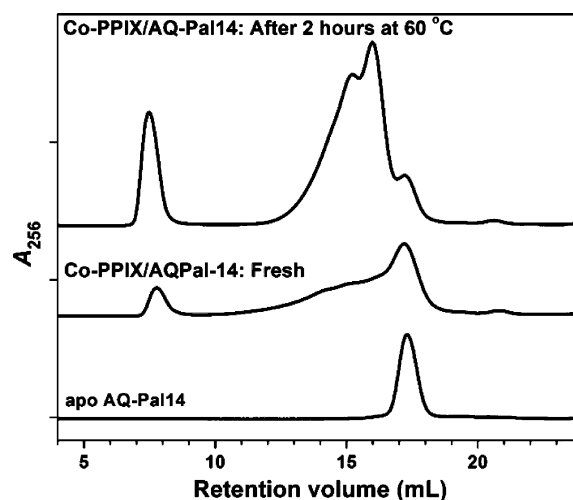


Figure 4. SEC profiles (Superdex 200) of apo AQ-Pal14 (bottom) and the Co-PPIX/AQ Pal14 reaction mixture after 0 (middle) and 2 (top) hours of incubation at 60 °C.

of molecular weights. UV-vis absorption scans of these newly formed species display a strong absorption band centered at 422–427 nm, indicating the presence of Co-PPIX. The top chromatogram in Figure 4 shows that, after 2 h of incubation at 60 °C, the apo-peptide population has decreased considerably, as judged by the diminished area of the corresponding elution peak at about 17.3 mL. At the same time, the populations of the higher molecular weight product species have all increased. At this point, the elution profile of the intermediate-sized species is clearly resolved into a shoulder and two peaks that elute at 14.2, 14.9, and 15.7 mL, respectively. Continued incubation at this temperature produced no further changes to the SEC elution profiles. Evaluation of signals from light scattering intensity and differential refractive index (Supporting Information, Figure S9) clearly indicates significant scattering due to the higher mass of the newly formed species as compared to the signals in the apo-peptide fraction. An estimation based on the elution time gives the masses in the range of 20–40 kDa and higher for the intermediate-sized species, which correspond to the assembly of two and more coiled coils.

DLS measurements were used to estimate the size distribution of the macromolecular aggregates in solution. The fraction eluting at 7–10 mL where the most intense scattering was observed (Supporting Information, Figure S9) was collected for

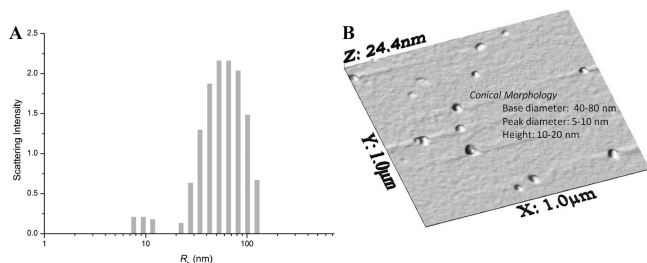


Figure 5. Conformational analysis of Co-PPIX/AQ-Pal14 assemblies by (A) dynamic light scattering of the highest molecular weight peak eluting from the SEC column and (B) atomic force microscopy of the assemblies prepared from 5% (v/v) DMF in H₂O (unbuffered).

the DLS analysis under the batch regime. Cumulant analysis of the correlation function of the scattering intensity collected for the earliest eluting peak shows a fairly high polydispersity index of 0.36 and a mean hydrodynamic radius of 50 ± 3 nm. The data processing under the regularization algorithm confirms this result showing that a major distribution spans in the range 20–100 nm and centers at about 55 nm (Figure 5A). Another distribution with a smaller R_h is likely the signature of intermediate-sized products.

Atomic force microscopy (AFM) of samples prepared from the reaction of AQ-Pal14 and Co-PPIX in 5% (v/v) DMF in H₂O (unbuffered) shows that this material forms conical structures having base diameters ranging from about 40–80 nm, peak diameters of 5–10 nm, and heights of 10–20 nm (Figure 5B) when deposited on a mica support. Under these conditions, similar structures were not observed from samples of either the peptide or the porphyrin alone, and it is seen that the CD spectrum of the peptide-porphyrin mixture is identical to those obtained in phosphate buffer shown in Figure S7 of the Supporting Information. These results suggest that the nanometer-scale structures result from the supramolecular assembly of the peptide-porphyrin tectons. It is noted that the species shown in Figure 5 are about 2-fold larger than ones made earlier using a Pt(ethylenediamine) center, which may reflect the inherent uncertainty of measuring dimensions in the plane of the mica support. Nevertheless, these structures have a similar overall shape to those previously described for the Pt-containing materials. This comparison suggests that the morphologies of these materials are likely dictated by the conformational properties of the three-stranded coiled-coil peptide AQ-Pal14 and not the coordination geometry of its metal component.

Formation of Millimeter-Scale Peptide-Porphyrin Rods from Phosphate Buffer. An interesting result was obtained when samples of the Co-PPIX/AQ-Pal14 tectons were prepared in 5% (v/v) DMF in 20 mM phosphate buffer (pH 7). The scanning electron micrographs (SEM) presented in Figure 6 show that the deposition of these materials onto conductive carbon tape produces one-dimensional rod-like materials having millimeter-scale lengths and micrometer-scale diameters. Whereas these materials can be seen by the naked eye, closer examination by SEM reveals that they are hierarchical in nature, existing as bundles of smaller rods each having diameters of $<2 \mu\text{m}$. These results are thus similar to our preliminary report of rod-like materials formed from the reaction of Co-PPIX with a related histidine-containing polypeptide which is known to form two-stranded coiled coils.⁵³ As this type of structure can be produced from peptides having different oligomerization motifs, it now appears that their formation is not driven by the self-assembly properties of the peptide.

To further investigate the nature of the rod-like peptide-porphyrin materials, it was found that they could only be formed

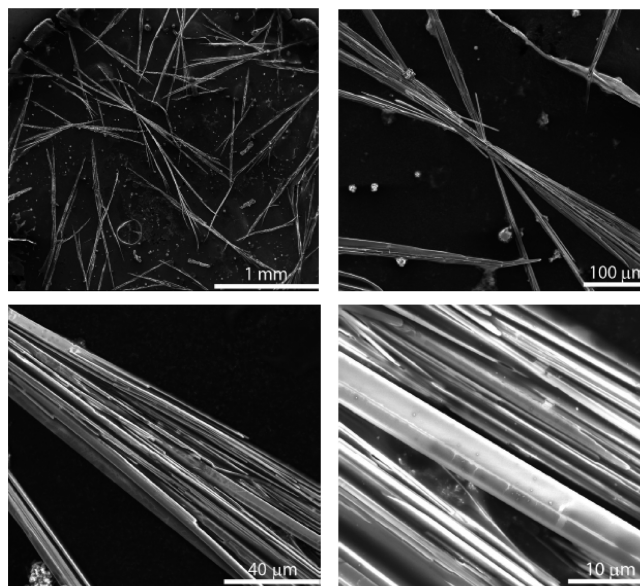


Figure 6. SEM images of Co-PPIX/AQ-Pal14 assemblies prepared from 5% (v/v) DMF in 20 mM phosphate buffer, pH 7, after evaporation from carbon conductive tape.

from phosphate buffer at pH 7 and not from HEPES buffer (pH 7), Tris buffer (pH 7), or pure H₂O. It was further observed that similar rod-like materials could not be formed from solutions of the peptide alone in the absence of buffer. However, similar structures were formed from Co-PPIX alone, but only when the pH of the phosphate buffer was lowered to just above 6. Together, the results suggest that formation of these materials involves either some type of porphyrin–phosphate interaction or perhaps from the crystallization of phosphate itself. In the former case, this would be similar to the situation previously reported for supramolecular arrays of tetra(4-carboxyphenyl)porphyrins in which adjacent porphyrin molecules were bridged by phosphate anions hydrogen-bonded to their peripheral carboxylic acid moieties.⁵⁴ This could translate into a situation where adjacent Co-PPIX molecules are organized by the hydrogen-bonding of phosphate anions to the propionic acid moieties of the porphyrin rings. Ongoing work is thus attempting to elucidate the detailed three-dimensional structure of these materials through X-ray crystallography to further understand the mechanism of their formation.

In the absence of such detailed structural information, the chemical composition of the peptide-porphyrin rods was analyzed by a variety of techniques. First, electron-dispersive X-ray analysis (EDX) was used to show the presence of cobalt, carbon, nitrogen, and large amounts of phosphorus and potassium in these materials (Supporting Information, Figure S10). Second, spectra obtained through confocal resonance Raman microscopy (Figure 7A) show strong signals within the region of 1300–1700 cm^{-1} which are identical to those seen in samples of Co-PPIX alone and compare favorably to those previously assigned to the in-plane vibrational modes of Co(III)-PPIX(pyridine)₂⁵⁵ and of Co(III)-PPIX measured in piperidine.⁵⁶ In these experiments, vibrations associated with the amide I band of the coiled-coil α -helix were not observed as they are presumably masked by the resonance-enhanced porphyrin signals. However, attenuated total reflectance microinfrared spectrometry of the rods do indeed show strong signals at 1650 and 1543 cm^{-1} (Figure 7B) that correspond to the amide I and amide II frequencies of α -helical polypeptides.⁵⁷ For comparison, Figure 7B also shows the IR spectrum taken of AQ-Pal14 alone deposited onto an

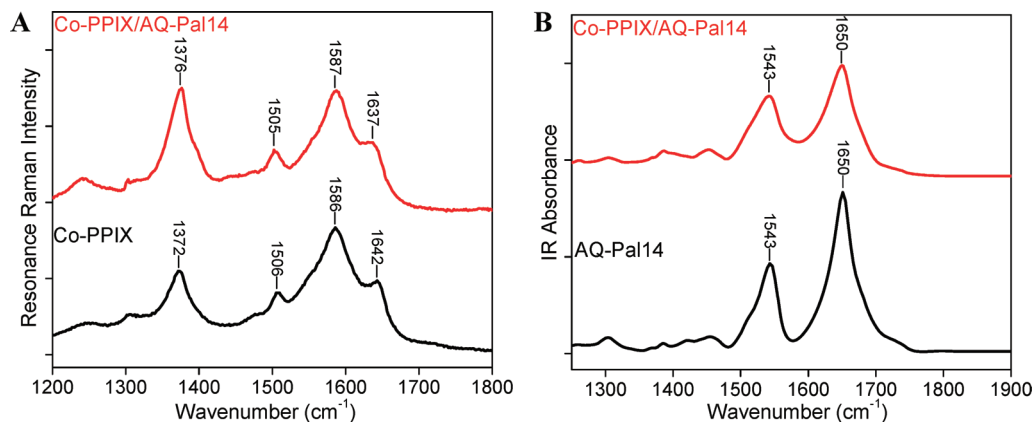
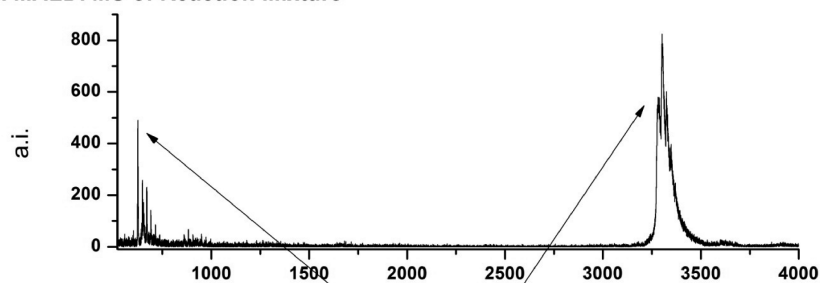


Figure 7. (A) Resonance Raman and (B) ATR-IR spectra of Co-PPIX/AQ-Pal14 assemblies prepared by evaporation from 5% (v/v) DMF in 20 mM phosphate buffer, pH 7. The top spectrum of each panel is from the Co-PPIX/AQ-Pal14 assemblies and the bottom spectrum is from either Co-PPIX or AQ-Pal14 alone.

A. MALDI MS of Reaction Mixture



B. MALDI MS of Isolated Fiber

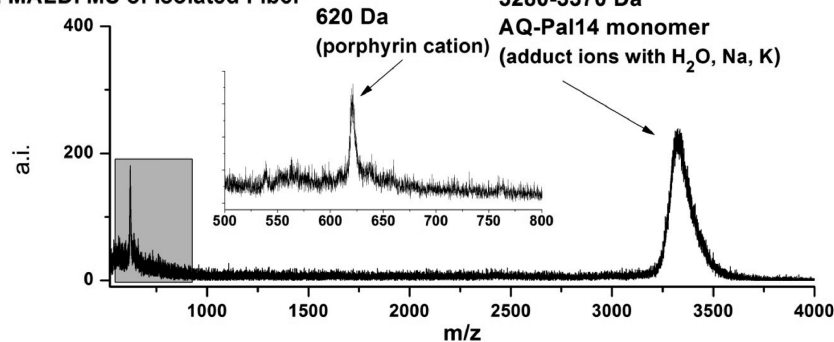


Figure 8. MALDI-MS spectra of (A) Co-PPIX/AQ-Pal14 reaction mixture and (B) Co-PPIX/AQ-Pal14 assemblies prepared from 5% (v/v) DMF in 20 mM phosphate buffer, pH 7.

aluminum foil support. It is noted, however, that the spatial resolution of the microinfrared experiment is insufficient to interrogate the composition of the peptide rods without also sampling some of the surrounding regions that might contain unreacted starting materials. Thus, MALDI-MS was used to confirm the chemical composition of this material. Figure 8A shows the MALDI-MS spectrum of an unreacted mixture of Co-PPIX and AQ-Pal14.

The spectrum consists of a signal located at $m/z = 620$ that corresponds to the $[\text{Co-PPIX}]^+$ cation in addition to a much broader signal at 3280–3370, which is assigned to various adducts of the AQ-Pal14 apo-peptide. Importantly, Figure 8B shows that the MALDI-MS spectrum of an isolated rod, carefully washed with methanol to remove the outer layers of material, contains the same components as found in the unreacted mixture. Together, the combination of Raman, IR, and MALDI-MS results demonstrate that the rod-like material shown in Figure 6 is indeed comprised of Co-PPIX and AQ-Pal14 but also contains a significant amount of phosphate ion. The assembly process of this material is presently unknown and the subject of further investigation.

Conclusions

The results presented above show how peptides and metal-porphyrins can be combined to make an interesting new class of materials having diverse three-dimensional morphologies depending on the conditions used in their preparation. Metal-peptide tecton units were prepared by binding individual chains of the self-assembling polypeptide AQ-Pal14 to the axial positions of Co-PPIX. This reaction produced a six-coordinate transition metal complex in which trimeric coiled-coil oligomerization domains were positioned on opposite faces of the porphyrin ring. The metal-peptide tectons were shown to assemble in solution via coiled-coil formation to produce globular materials having diameters less than 100 nm when prepared in unbuffered water, as shown by both DLS and AFM experiments. It is interesting to note that the morphology of these materials is very similar to that of the previously studied Pt/AQ-Pal14 system whose tectons were prepared by coordinating AQ-Pal14 units to the *cis* positions of a square-planar metal complex. This similarity in morphology occurs despite significant differences in the coordination geometries of their constitu-

ent metal sites to indicate that their structures are likely driven by the conformational properties of the peptide. In contrast, when samples were prepared from phosphate buffer, millimeter-scale peptide rods were formed upon evaporation, which might possibly arise from hydrogen-bond interactions occurring between the propionic acid moieties of the metalloporphyrin ring and phosphate ion or perhaps from the crystallization of the phosphate itself. In any case, it is apparent that the formation of these structures does not rely on the assembly properties of the peptide. Together, these results highlight the diversity of materials that can be prepared upon reacting simple inorganic coordination compounds with self-assembling polypeptides, and it is anticipated that continued study of these materials will further our abilities to produce peptide-based materials having rationally controlled morphologies for use as next-generation materials for medicine and technology.

Acknowledgment. This work was supported by NSF Grant Nos. CHE-0455441 (M.Y.O.) and CHE-0964806 (D.L.T.), ACS-PRF Grant No. 34901-AC (M.Y.O.), and NIH Grant No. RR022200 (B.D.). The authors thank Professor Phil Castellano for use of the Raman microscope and Professor Arun Nadarajah for access to the instrumentation at the Center for Materials and Sensor Characterization at the University of Toledo.

Supporting Information Available. Thermal denaturation curve of AQ-Pal14; SEC-MALS, DLS correlogram, regularization analysis, and AUC analysis of the AQ-Pal14 apopeptide; UV-vis spectra of metalation reactions; circular dichroism spectrum of Co-PPIX/AQ-Pal14; EXAFS data fits, and EDX analysis of Co-PPIX/AQ-Pal14 fibers. This material is available free of charge via the Internet at <http://pubs.acs.org>.

References and Notes

- Gazit, E. *Chem. Soc. Rev.* **2007**, *36*, 1263–1269.
- Pepe-Mooney, B. J.; Fairman, R. *Curr. Opin. Struct. Biol.* **2009**, *19*, 483–494.
- Woolfson, D. N.; Ryadnov, M. G. *Curr. Opin. Chem. Biol.* **2006**, *10*, 559–567.
- Zhang, S. G. *Nat. Biotechnol.* **2003**, *21*, 1171–1178.
- Ellis-Behnke, R. G.; Liang, Y. X.; You, S. W.; Tay, D. K. C.; Zhang, S. G.; So, K. F.; Schneider, G. E. *Proc. Natl. Acad. Sci. U.S.A.* **2006**, *103*, 5054–5059.
- Emerich, D. F.; Thanos, C. G. *Curr. Opin. Mol. Ther.* **2008**, *10*, 132–139.
- Mart, R. J.; Osborne, R. D.; Stevens, M. M.; Ulijn, R. V. *Soft Matter* **2006**, *2*, 822–835.
- Tsurkan, M. V.; Ogawa, M. Y. *Biomacromolecules* **2007**, *8*, 3908–3913.
- Tsurkan, M. V.; Ogawa, M. Y. *Inorg. Chem.* **2007**, *46*, 6849–6851.
- Tsurkan, M. V.; Ogawa, M. Y. *Chem. Commun.* **2004**, 2092–2093.
- Hong, J.; Kharenko, O. A.; Ogawa, M. Y. *Inorg. Chem.* **2006**, *45*, 9974–9984.
- Kharenko, O. A.; Kennedy, D. C.; Demeler, B.; Maroney, M. J.; Ogawa, M. Y. *J. Am. Chem. Soc.* **2005**, *127*, 7678–7679.
- Kharenko, O. A.; Ogawa, M. Y. *J. Inorg. Biochem.* **2004**, *98*, 1971–1974.
- Dublin, S. N.; Conticello, V. P. *J. Am. Chem. Soc.* **2008**, *130*, 49–51.
- Ghosh, S.; Verma, S. *Tetrahedron Lett.* **2007**, *48*, 2189–2192.
- Kasotakis, E.; Mossou, E.; Adler-Abramovich, L.; Mitchell, E. P.; Forsyth, V. T.; Gazit, E.; Mitraki, A. *Biopolymers* **2009**, *92*, 164–172.
- Matsumura, S.; Uemura, S.; Mihara, H. *Supramol. Chem.* **2006**, *18*, 397–403.
- Przybyla, D. E.; Chmielewski, J. *J. Am. Chem. Soc.* **2008**, *130*, 12610–12611.
- Salgado, E. N.; Lewis, R. A.; Faraone-Mennella, J.; Tezcan, F. A. *J. Am. Chem. Soc.* **2008**, *130*, 6082–6084.

- Scotter, A.; Guo, M.; Tomczak, M.; Daley, M.; Campbell, R.; Oko, R.; Bateman, D.; Chakrabarty, A.; Sykes, B.; Davies, P. *BMC Struct. Biol.* **2007**, *7*, 63.
- Yang, H.; Pritzker, M.; Fung, S. Y.; Sheng, Y.; Wang, W.; Chen, P. *Langmuir* **2006**, *22*, 8553–8562.
- Kerman, K.; Kraatz, H. B. *Angew. Chem., Int. Ed.* **2008**, *47*, 6522–6524.
- Crick, F. H. C. *Acta Crystallogr.* **1953**, *6*, 689–697.
- Bromley, E. H. C.; Channon, K.; Moutevelis, E.; Woolfson, D. N. *ACS Chem. Biol.* **2008**, *3*, 38–50.
- Cohen, C.; Parry, D. A. D. *Proteins: Struct., Funct., Bioinf.* **1990**, *7*, 1–15.
- Hodges, R. S. *Biochem. Cell Biol.* **1996**, *74*, 133–154.
- Harbury, P. B.; Zhang, T.; Kim, P. S.; Alber, T. *Science* **1993**, *262*, 1401–1407.
- Armstrong, C. T.; Boyle, A. L.; Bromley, E. H. C.; Mahmoud, Z. N.; Smith, L.; Thomson, A. R.; Woolfson, D. N. *Faraday Discuss.* **2009**, *143*, 305–317.
- Frissen, B. J. *Appl. Opt.* **2001**, *40*, 4087–4091.
- Brookes, E.; Demeler, B. *Colloid Polym. Sci.* **2008**, *286*, 139–148.
- Brookes, E.; Cao, W. M.; Demeler, B. *Eur. Biophys. J.* **2010**, *39*, 405–414.
- Brookes, E.; Demeler, B.; Rosano, C.; Rocco, M. *Eur. Biophys. J.* **2010**, *39*, 423–435.
- Wagschal, K.; Tripet, B.; Lavigne, P.; Mant, C.; Hodges, R. S. *Protein Sci.* **1999**, *8*, 2312–2329.
- Horcas, I.; Fernandez, R.; Gomez-Rodriguez, J. M.; Colchero, J.; Gomez-Herrero, J.; Baro, A. M. *Rev. Sci. Instrum.* **2007**, *78*.
- Periyannan, G. R.; Costello, A. L.; Tierney, D. L.; Yang, K. W.; Bennett, B.; Crowder, M. W. *Biochemistry* **2006**, *45*, 1313–1320.
- Webb, S. M. *Phys. Scr.* **2005**, *T115*, 1011–1014.
- Ankudinov, A. L.; Ravel, B.; Rehr, J. J.; Conradson, S. D. *Phys. Rev. B* **1998**, *58*, 7565–7576.
- Su, J. Y.; Hodges, R. S.; Kay, C. M. *Biochemistry* **1994**, *33*, 15501–15510.
- Kornilova, A. Y.; Wishart, J. F.; Xiao, W. Z.; Lasey, R. C.; Fedorova, A.; Shin, Y. K.; Ogawa, M. Y. *J. Am. Chem. Soc.* **2000**, *122*, 7999–8006.
- Wen, J.; Arakawa, T.; Philo, J. S. *Anal. Biochem.* **1996**, *240*, 155–166.
- Zaytsev, D.; Ni, S.; Kennedy, M. A.; Ogawa, M. Y. unpublished results, 2010.
- Dokuzovic, Z.; Ahmeti, X.; Pavlovic, D.; Murati, I.; Asperger, S. *Inorg. Chem.* **1982**, *21*, 1576–1581.
- Hagarman, A.; Duitch, L.; Schweitzer-Stenner, R. *Biochemistry* **2008**, *47*, 9667–9677.
- Mizutani, T.; Ema, T.; Yoshida, T.; Renne, T.; Ogoshi, H. *Inorg. Chem.* **1994**, *33*, 3558–3566.
- Tamiaki, H.; Unno, S.; Takeuchi, E.; Tameshige, N.; Shinoda, S.; Tsukube, H. *Tetrahedron* **2003**, *59*, 10477–10483.
- Kokona, B.; Kim, A. M.; Roden, R. C.; Daniels, J. P.; Pepe-Mooney, B. J.; Kovacic, B. C.; de Paula, J. C.; Johnson, K. A.; Fairman, R. *Biomacromolecules* **2009**, *10*, 1454–1459.
- Kovacic, B. C.; Kokona, B.; Schwab, A. D.; Twomey, M. A.; de Paula, J. C.; Fairman, R. *J. Am. Chem. Soc.* **2006**, *128*, 4166–4167.
- McAllister, K. A.; Zou, H. L.; Cochran, F. V.; Bender, G. M.; Senes, A.; Fry, H. C.; Nanda, V.; Keenan, P. A.; Lear, J. D.; Saven, J. G.; Therien, M. J.; Blasie, J. K.; DeGrado, W. F. *J. Am. Chem. Soc.* **2008**, *130*, 11921–11927.
- Pasternack, R. F.; Giannetto, A.; Pagano, P.; Gibbs, E. J. *J. Am. Chem. Soc.* **1991**, *113*, 7799–7800.
- Brucker, E. A.; Olson, J. S.; Phillips, G. N.; Dou, Y.; IkedaSaito, M. *J. Biol. Chem.* **1996**, *271*, 25419–25422.
- Lauher, J. W.; Ibers, J. A. *J. Am. Chem. Soc.* **1974**, *96*, 4447–4452.
- Zahran, Z. N.; Chooback, L.; Copeland, D. M.; West, A. H.; Richter-Addo, G. B. *J. Inorg. Biochem.* **2008**, *102*, 216–233.
- Carvalho, I. M. M.; Ogawa, M. Y. *J. Braz. Chem. Soc.* **2010**, *21*, 1390–1394.
- George, S.; Goldberg, I. *Cryst. Growth Des.* **2006**, *6*, 755–762.
- Woodruff, W. H.; Sprio, T. G.; Yonetani, T. *Proc. Natl. Acad. Sci. U.S.A.* **1974**, *71*, 1065–1069.
- Woodruff, W. H.; Adams, D. H.; Spiro, T. G.; Yonetani, T. *J. Am. Chem. Soc.* **1975**, *97*, 1695–1698.
- Pelton, J. T.; McLean, L. R. *Anal. Biochem.* **2000**, *277*, 167–176.